Lasers in Eng., Vol. 41, pp. 205–217
Reprints available directly from the publisher
Photocopying permitted by license only

Laser-assisted Four Point Bending of Aluminium Sheet

Q. PENG*

[1]*Institute of Mechanics, Chinese Academy of Sciences, No. 15, Beisihuanxi Road, Beijing 100190, China*

Laser-assisted pre-stress forming is a technology for the manufacturing an integrally stiffened panel. To investigate the thermo-mechanical mechanism for such forming method, experiment on laser-assisted four-point bending an AA6061-T6 aluminium alloy sheet is carried out. A three-dimensional (3-D) finite element method (FEM) simulation is conducted and verified with the experiment in aspects of both temperature histories and force-displacement curve. During forming process, the sample is bent *via* four point bending elastically and then heated with a continuous wave (CW) Nd:YAG laser system in a controllable manner. Since material yield strength decreases with an increasing temperature locally, pre-loaded elastic strain is partially converted into plastic strain, and elastic strain energy is dissipated into plastic work. In this paper, the forming mechanism is studied by analysing the coupled thermo-structural field. According to the final shape by simulation, the spring-back ratio is 78.0% (76.0% by experiment), and the energy dissipation rate is 33.5%.

Keywords: Nd:YAG laser, AA6061-T6 aluminium alloy, finite element method (FEM), laser-assisted, four point bending, pre-stress forming, spring-back

1 INTRODUCTION

Integrally stiffened panel of airplane is widely used for aircraft because of its remarkable structural strength and stiffness [1]. In comparison with traditional aircraft wing-panel, integrally stiffened panels can significantly prolong the life span of an aircraft and reduce the weight; however, forming of

*Corresponding author: E-mail: qpeng@imech.ac.cn

integrally stiffened panel of airplane brings a challenge to the aeronautical manufacturing technology; the integrally stiffened panel is hard to be bent directly. Traditionally, forming technologies such as three point bending and four point bending are used for the forming of such stiffened structures. During bending process, to achieve a desired plastic deformation, a remarkable amount of elastic strain energy is stored in the part, as generally indicated by a phenomenon of large spring-back, which is a key to the geometric accuracy of forming a mechanical part [2]; consequently, the accuracy of forming is limited. On the other hand, applying bending loads could induce structural failures such as cracking and buckling especially in the regions of stress concentration around stiffeners [3–5]. Such difficulty, however, can be overcome if the elastic strain energy within the structure can be dissipated into plastic work *via* softening the work piece by selective heating in a specific area.

Selective heating can be implemented with many kinds of energy source such as laser power, electronic beam, and even flame. In the present study, laser power is used. Bending with laser scanning is performed according to the following procedures, which are also illustrated in Figure 1:

(i) Four point bend the work piece to a deformation state in which the strain energy is elastic;
(ii) Maintain the deformation state and heat at specific regions by laser scanning; and
(iii) Remove all the external loads after the work piece is cooled down to room temperature.

When the sample is heated by laser scanning the material yield strength in the heated region decreases. The stored elastic energy in Procedure (i)

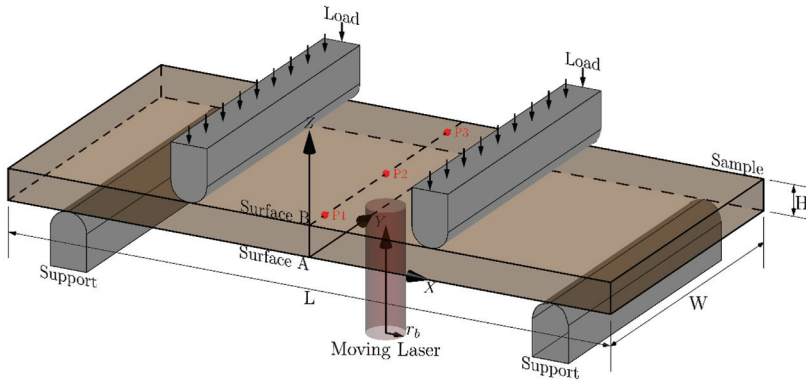

FIGURE 1
Schematic diagram showing four point bending with laser forming.

is thus partially dissipated into the plastic work; consequently, a relatively smaller spring-back will further be produced in Procedure (iii) than that by common bending procedures. In other words, the accuracy of forming is enhanced.

In this paper an experiment on laser-assisted four point bending is conducted. Then a finite element method (FEM) simulation is performed to analysis the forming mechanisms.

2 EXPERIMENTAL DETAILS

The material used in the experiment is AA6061-T6 aluminium alloy sheet. Table 1 lists the specification for geometrical dimensions and laser parameters. In order to increase energy absorption, the sample is coated with a layer of graphite ink.

The experimental procedures included three parts: mechanical loading; laser scanning/cooling; and mechanical unloading. During mechanical loading, the sample is placed and bent with a multifunctional material test machine (GP-TS2000HM; GoPoint Technology, Inc.). The distance between two punch noses is 36 mm, and the distance between two supports is 80 mm. The laser (lab-made) used was a continuous wave (CW) Nd:YAG laser emitting a top-hat beam at 1064nm. The Nd:YAG laser beam was scanning on the bottom side (Surface A) of the sample along width direction (y+), as Figure 1 illustrates. After the sample cooled down naturally to room temperature, the loading force is removed and then the sample is finally formed. During the experiment, the loading force and the displacement of the punch nose are logged. Temperature histories of $P1(0,0.1W,H)$, $P2(0,0.5W,H)$ and $P3(0,0.9W,H)$ are measured with Type K thermocouples and a data logger (8430–20; HIOKI, Ltd.).

TABLE 1
Parameters used in the experiments.

Parameter	Value
Sample length (L)	100 mm
Sample width (W)	48 mm
Sample thickness (H)	1 inch
Laser power (P)	140 W
Absorptivity (A)	0.7
Laser beam radius (r_b)	3 mm
Laser scanning speed (V)	0.5 mm/s

3 NUMERICAL SIMULATION METHOD

In the present numerical simulation, the commercial finite element program ABAQUS is used. Since the heat generation by deformation is negligible in comparison with the heat flow by the laser beam, a sequentially coupled field technique can be adopted. This essentially means that stress field hardly has influence on temperature field, and hence both temperature field and stress field can be solved in sequence [6, 7].

The transient temperature field is determined based on heat transfer equation. The laser beam is modelled as a moving heat flux, which is implemented with ABAQUS DFLUX subroutine, applied on the bottom surface of the sample. To simplify the analysis, three assumptions are presumed to solve the thermal field:

(i) The laser intensity distribution is uniform;
(ii) Only convection ($h = 60\,\mathrm{W/m^2K}$) is considered; and
(iii) Changes of physical properties with temperature can be linear interpolated, as shown in Figure 2 and Figure 3.

The governing equation for heat conduction is expressed as

$$\rho c \frac{\partial T}{\partial t} = \nabla(k \nabla T) \tag{1}$$

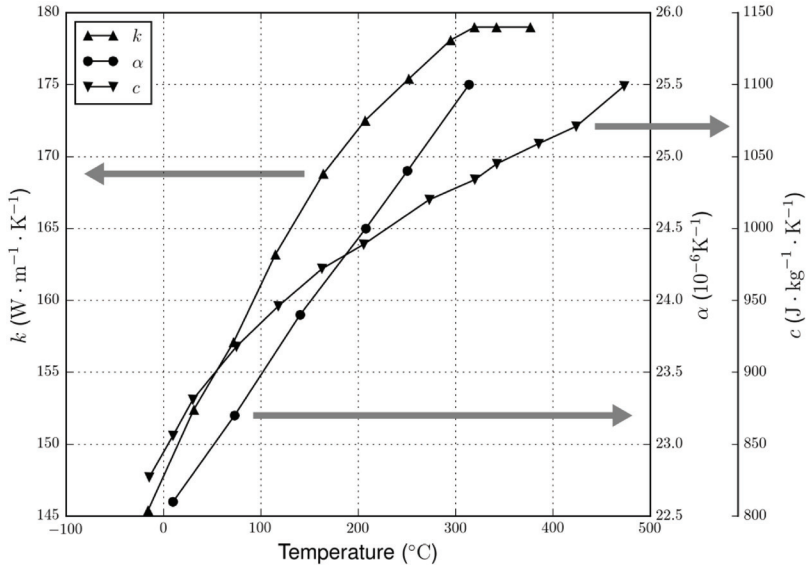

FIGURE 2
Thermal properties used in the FEM simulation.

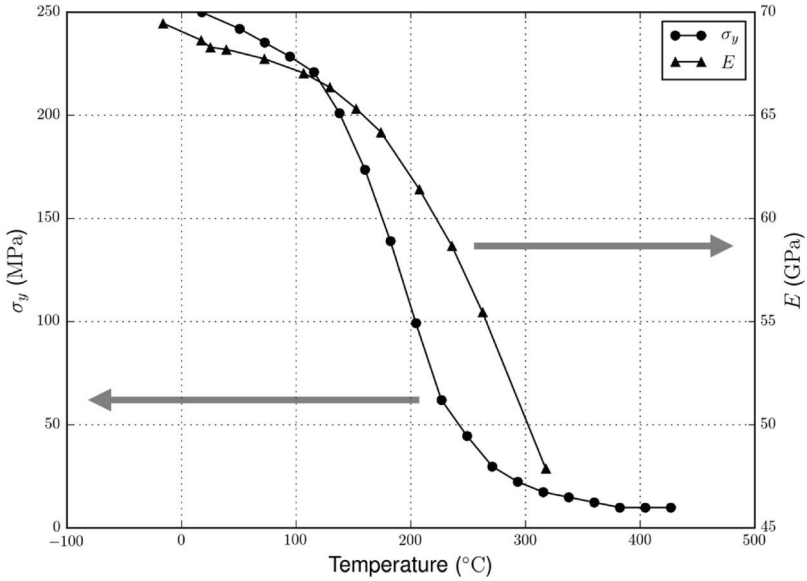

FIGURE 3
Mechanical properties used in the FEM simulation.

where ρ is the density, c the specific heat, T the temperature and t is the time. The moving heat flux generated by the laser scanning is expressed as

$$I = \begin{cases} \dfrac{AP}{\pi r^2} & \sqrt{(x - x_o(t))^2 + (y - y_o(t))^2} < r \\ 0 & \sqrt{(x - x_o(t))^2 + (y - y_o(t))^2} \geq r \end{cases} \tag{2}$$

where A is the absorption coefficient, P the power of laser beam, r the radius of laser spot, and $x_0(t)$, $y_0(t)$ the coordinates of the centre of the laser spot in global coordinate system at time t.

Time scale of stress in response to thermal field is negligible, compared to that of heat transfer; consequently, a quasi-static approach can be adopted in structural field analysis. The following are assumed to calculate the structural field [8–13]:

(i) The material is isotropic;
(ii) The material is elastic-perfectly plastic;
(iii) The material is incompressible when plastically deformed;
(iv) Strain rate effects are neglected; and
(v) The yield function is assumed as [14]

$$f = \frac{1}{2} s_{ij} s_{ij} - k_c(T)^2 \tag{3}$$

where s_{ij} is the deviatoric stress and k_c is the temperature dependent yield stress of material in pure shear. The relation between strain ε_{ij} and stress σ_{ij} can be expressed as [14]

$$\dot{\varepsilon}_{ij} = \frac{1+v}{E}\dot{\sigma}_{ij} - \delta_{ij}\frac{v}{E}\dot{\sigma}_{kk} + (1-g)\,\lambda\left(\sigma_{ij} - \delta_{ij}\frac{\sigma_{kk}}{3}\right) + \sigma_{ij}\alpha\dot{T} \tag{4}$$

where

$$\begin{cases} \lambda = 0 & \text{if } \frac{1}{2}s_{ij}s_{ij} < k_c^2, \text{ or if } \frac{1}{2}s_{ij}s_{ij} = k_c^2 \text{ and } s_{ij}\dot{s}_{ij}^E \le 0 \\ \lambda = \frac{s_{ij}\dot{e}_{ij}}{2k_c^2} \text{ and } s_{ij}\dot{s}_{ij} = 0 & \text{if } \frac{1}{2}s_{ij}s_{ij} = k_c^2 \text{ and } s_{ij}\dot{s}_{ij}^E \ge 0 \end{cases} \tag{5}$$

in which δ_{ij} is the Kronecker delta and e_{ij} is the deviatoric strain. In Equation (4) g vanishes in the plastic state and equals to unity in the elastic state:

$$g = \begin{cases} 1 & \text{if } \frac{1}{2}s_{ij}s_{ij} < k_c^2, \text{ or if } \frac{1}{2}s_{ij}s_{ij} = k_c^2 \text{ and } s_{ij}\dot{s}_{ij}^E \le 0 \\ 0 & \text{if } \frac{1}{2}s_{ij}s_{ij} = k_c^2 \text{ and } s_{ij}\dot{s}_{ij}^E \ge 0 \end{cases} \tag{6}$$

Because of the symmetry only half a model is necessary. In such case, necessary constraints are applied on certain geometric features of the geometry model, including a symmetry constraint on the symmetry plane. Figure 4

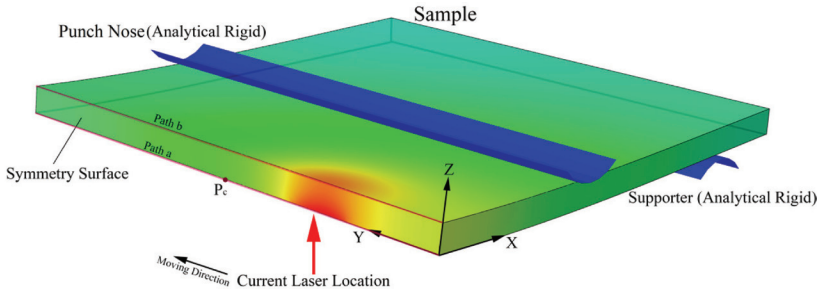

FIGURE 4
Symmetric model for the FEM simulation.

TABLE 2
Stages in the FEM simulation.

Time (seconds)	Stage
$t = 0$ to 10	1: Mechanical loading
$t = 10$ to 118	2: Laser heating
$t = 118$ to 740	3: Cooling
$t = 740$ to 750	4: Unloading

shows the symmetrical FEM model used for simulation. The punch nose and support are modelled as analytical rigid bodies. During the simulation, contact pairs are established for modelling the loading process. Table 2 lists the four main stages during the whole forming process.

4 RESULTS AND DISCUSSION

To validate the numerical model, Figure 5 plots both the computed and experimental temperature histories at point *P*1, *P*2, and *P*3, respectively, which shows a consistency of the numerical results and the experimental measure-

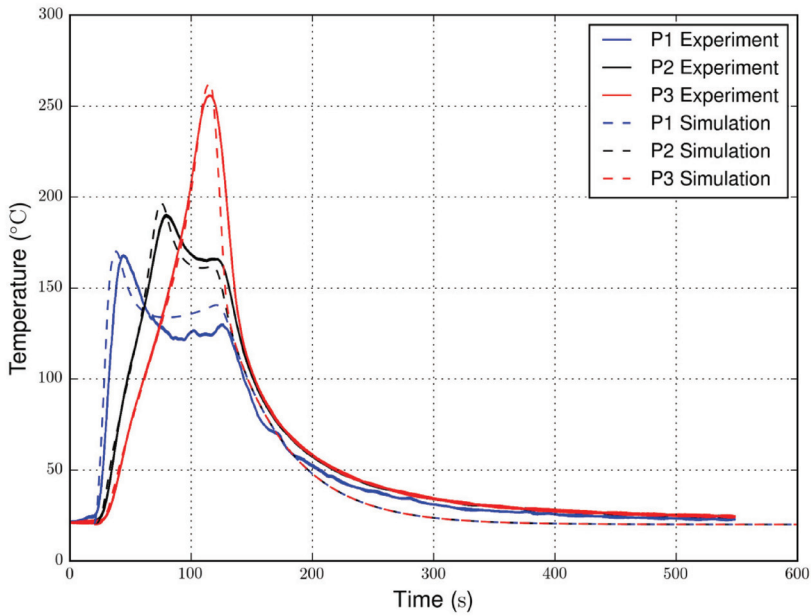

FIGURE 5
Measured and FEM simulated temperature histories at locations *P*1, *P*2 and *P*3.

ments within a margin of error. Such minor differences may result from the thermal contact between the punch noses/the supporters and the sample, which is neglected in the presented simulation. On the other hand, in the experimental situation, differing from the numerical model, the absorptivity may be also temperature dependent. Figure 6 plots both the simulated and experimental force-displacement curve of the punch nose. With admissible errors, both the thermal and the mechanical models are consistent with experimental data and thus verified. With the force-displacement curve, a spring-back ratio can be defined as

$$\gamma = \frac{\omega_0 - \omega_1}{\omega_0} \tag{7}$$

where ω_0 is the deflection during Procedure (i), and ω_1 is the residual deflection at the punch noses. The experimental and numerical spring-back ratio at the punch noses is, respectively, 76.0% and 78.0%.

When the sample is heated with a moving laser beam, the generation of plastic strain energy is a result of the decreasing in material yield strength, which is locally determined by the maximal temperature. Figure 7 shows the local maximal temperature of each point on Path (a) on Surface A and Path (b) on Surface B, illustrated in Figure 1 and Figure 4. The peak temperature

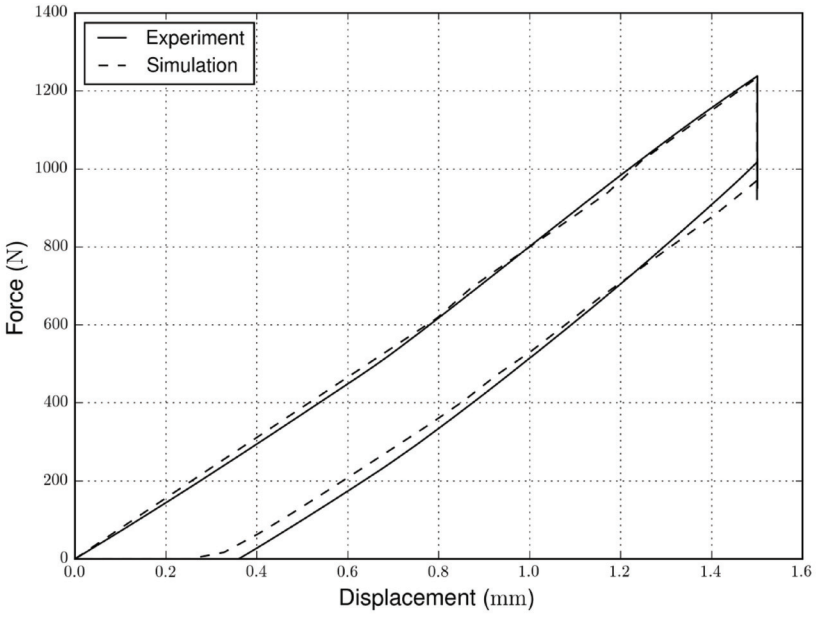

FIGURE 6
Measured and FEM simulated force-displacement curve of the punch nose.

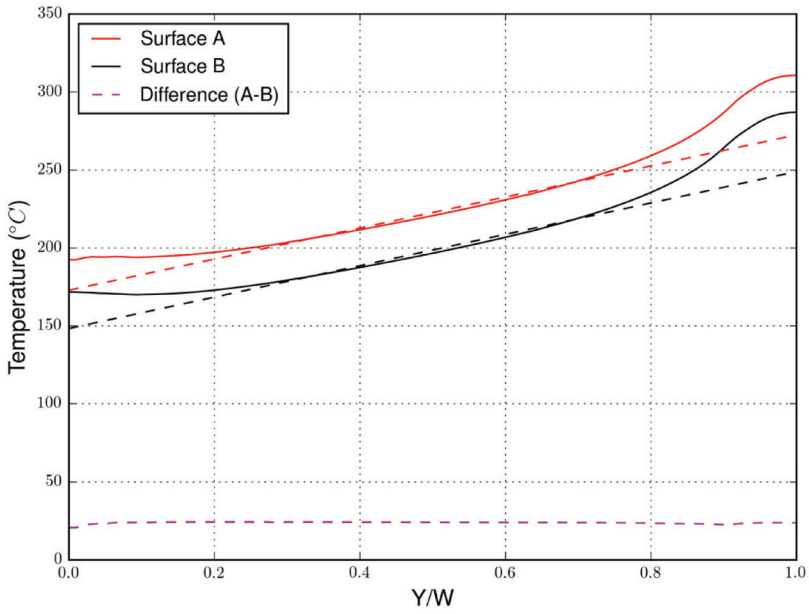

FIGURE 7
Peak temperature distributions at Surface A and Surface B along Path (a) and Path (b).

tends to increase along *y*-axis. As the laser spot moves to the centre, dynamic equilibrium is hard to be established, accounting for the linear increase in the interval [0.2,0.8], indicated by linearly fitted dash lines. On the other hand, the peak temperature deviated from the fitted lines near both edges. This results from the effects of edge overheating [15]. The difference of the peak temperature between Path (a) and Path (b) is also plotted in Figure 7, which is constantly about 25ºC and much lower than the temperature gradient necessary in laser bending a sheet metal [16]. This means that, unlike the processing strategy in laser forming, an even temperature distribution cross the sheet thickness could lead to a better energy dissipation, and hence a suppression of the spring-back ratio.

Figure 8 shows the distribution of the equivalent plastic strain after forming, which indicates that the deformation induced by laser heating is concentrated within the laser-scanned area, although the plastic deformation may occur outside such region with a relatively much lower magnitude. On the other hand, the plastic deformation is also concentrated near the exiting edge of laser beam. This means edge distortion will take place. Based on displacement field of the mid-plane of the sample, a Gaussian curvature field is calculated. For bending along a single direction, the Gaussian curvature should be exactly zero. Figure 9 shows that intense distortion takes place around the exiting edge.

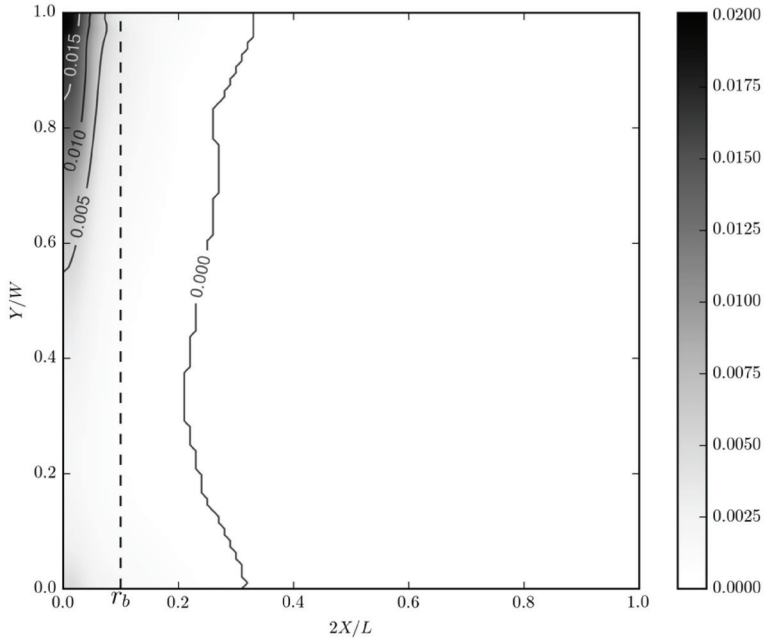

FIGURE 8
Contour of the distribution of equivalent plastic strain on Surface A.

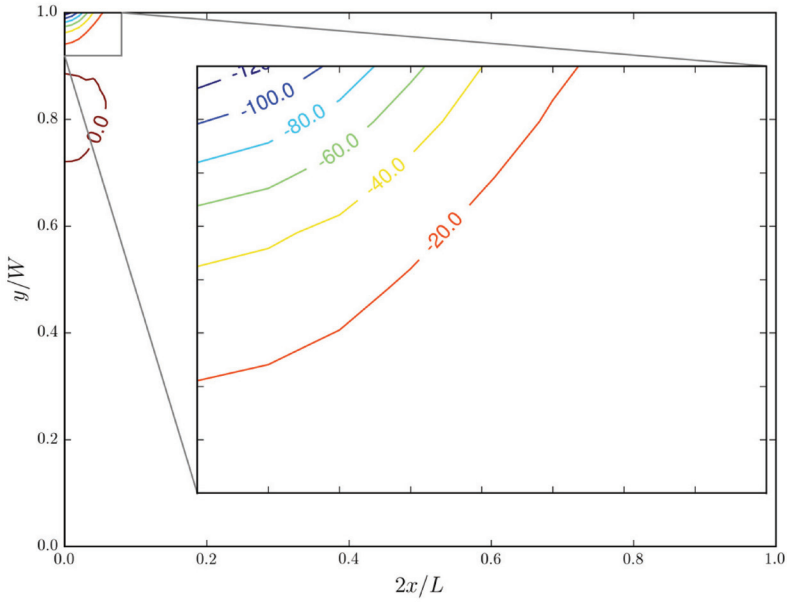

FIGURE 9
Contour of the distribution of Gaussian curvature on the sample's mid-plane.

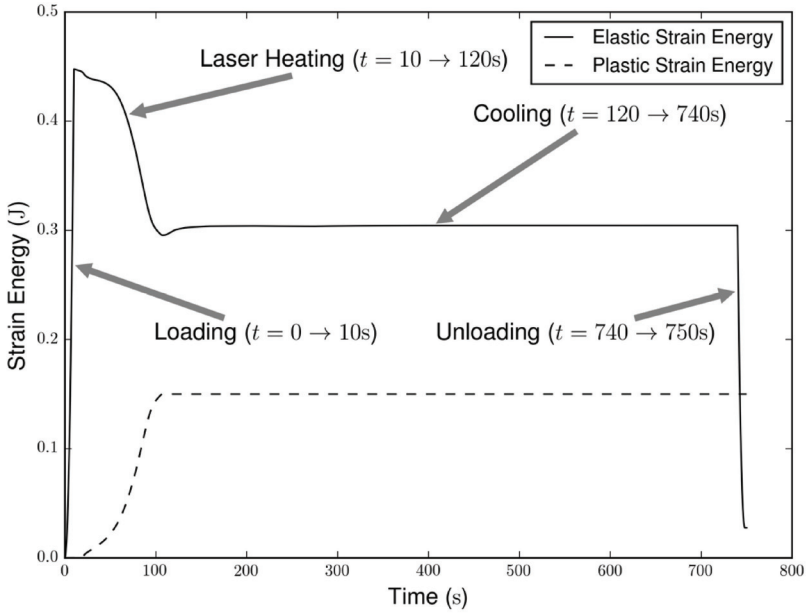

FIGURE 10
Variations of the elastic and plastic strain energy during overall forming process.

In aspect of energy balance, during the mechanical loading process, elastic strain energy is stored in the sample, and absolutely no plastic work is produced. While the sample is heated with laser, the elastic strain energy is dissipated into the plastic work, shown by Figure 10. During cooling procedure, both the elastic energy and the plastic energy remain unchanged. The unloading procedure shows a partial release of the elastic strain energy, the remainder of which is stored as an unevenly distributed residual stress. In the overall forming process, one can define an energy dissipation ratio as

$$\xi = \frac{E_p}{E_{e0}} \tag{8}$$

where E_{e0} is the pre-loaded elastic strain energy, and E_p is the plastic work. In this case the energy dissipation value is 33.5%.

5 CONCLUSIONS

A three-dimensional (3-D) thermo-mechanical finite element method (FEM) model is established to analyse the mechanism of the laser-assisted pre-stress

forming. The simulation results were verified with the experiments. In aspect of the temperature histories and force-displacement curve, the simulated results agree with those measured in experiment. The forming mechanism is a contraction of material yield surface due to temperature elevation and peak temperature distribution. Pre-loaded elastic strain is partially converted into plastic strain, and elastic strain energy is dissipated into plastic work. The peak temperature along laser scanning path is distributed unevenly because of the low scanning speed of the laser, which is unable to establish a dynamical equilibrium. The plastic strain is concentrated in the rear of the scanning path and within a length of laser radius in the x-direction. The Gaussian curvature distribution indicates that edge distortion exists near the exiting edge due to the exceptionally elevated temperature in that area. According to the final formed shape, the spring-back ratio is 78.0% (76.0% by experiment), and the dissipation rate of the elastic strain energy into plastic work is 33.5%.

ACKNOWLEDGEMENT

This work was supported by the National Natural Science Foundation of China through Grant No. 11102210.

NOMENCLATURE

A	Absorption coefficient, <1
c	Specific heat (J/kgK)
E_{e0}	Pre-loaded elastic strain energy (J)
E_p	Plastic work (J)
e_{ij}	Deviatoric strain tensor
h	Heat transfer coefficient (W/m^{2}K)
I	Heat flux (W/m^2)
k	Thermal conductivity (W/mK)
k_c	Yield stress of material in pure shear (Pa)
P	Power of laser beam (W)
r	Radius of laser beam (m)
s_{ij}	Deviatoric stress tensor (Pa)
t	Time (seconds)
T	Temperature (K)

Greek symbols

α	Coefficient of thermal expansion (K^{-1})
γ	Spring-back ratio
δ_{ij}	Kronecker delta
ε_{ij}	Strain tensor

ν Poisson's ratio
ξ Energy dissipation ratio
ρ Density of material (kg/m^3)
σ_{ij} Stress tensor (Pa)
ω Deflection (m)

REFERENCES

[1] McQueen J.C., McClaren S.W. and Martin A.P. Integrally formed structures. A new stiffened panel concept. *Journal of Aircraft* **7**(6) (1970), 563–566.

[2] Zhang X.J. and Zhou X.B. Simulation of springback in sheet metal forming. *Journal of Plasticity Engineering* **6**(3) (1999), 56–62.

[3] Liu J.S., Zhang S.H., Zeng Y.S. and Li Z.Q. Ren Li-Mei. Simulation of incremental forming on integral panel skin with grid-type ribs. *Material Science and Technology* **12**(5) (2004), 515–517.

[4] Patel S.N., Datta P.K. and Sheikh A.H. Dynamic instability analysis of stiffened shell panels subjected to partial edge loading along the edges. *International Journal of Mechanical Sciences* **49**(12) (2007), 1309–1324.

[5] Hosseini-Toudeshky H., Loughlan J. and Kharazi M. The buckling characteristics of some integrally formed bead stiffened composite panels. *Thin-Walled Structures* **43**(4) (2005), 629–645.

[6] Hsieh H.S. and Lin J. Study of the buckling mechanism in laser tube forming with axial preloads. *International Journal of Machine Tools & Manufacture* **45**(12) (2005), 1368–1374.

[7] Guan Y-J., Yuan G-P., Sun S. and Zhao G-Q. Process simulation and optimization of laser tube bending. *The International Journal of Advanced Manufacturing Technology* **65**(1–4) (2013), 333–342.

[8] Shi Y.J., Yao Z.Q., Shen H. and J. Hu. Research on the mechanisms of laser forming for the metal plate. *International Journal of Machine Tools & Manufacture* **46**(12) (2006), 1689–1697.

[9] Lee K.C. and Lin J. Transient deformation of thin metal sheets during pulsed laser forming. *Optics & Laser Technology* **34**(8) (2002), 639–648.

[10] Hsieh H.S. and Lin J. Thermal-mechanical analysis on the transient deformation during pulsed forming. *International Journal of Machine Tools & Manufacture* **44**(2) (2004), 191–199.

[11] Hao N. and Li L. Finite element analysis of laser tube bending. *Applied Surface Science* **208–209** (2003), 432–436.

[12] Hao N. and Li L. An analytical model for laser tube bending. *Applied Surface Science* **208–209** (2003), 437–441.

[13] Safdar S., Li L., Sheikh M.A. and Liu Z. Finite element simulation of laser tube bending: Effect of scanning schemes on bending angle, distortions and stress distribution. *Optics & Laser Technology* **39**(6) (2007), 1101–1110.

[14] Boley B.A. and Weiner J.H. *Theory of Thermal Stresses*. New York: John Wiley and Sons. 1960.

[15] Lambiase F., Di Ilio A. and Paoletti A. An experimental investigation on passive water cooling in laser forming process, *International Journal of Advanced Manufacturing Technology* **64**(5) (2013), 829–840.

[16] Shen H., Shi Y.J., Yao Z.Q. and Hu J. An analytical model for estimating deformation in laser forming, *Computational Materials Science* **37**(4) (2006), 593–598.